J MATER SCI **41** (2006) 661–674

The effects of crystallography on grain-boundary migration in alumina

JEFFREY K. FARRER
Department of Physics and Astronomy, Brigham Young University, Provo, UT 84602

C. BARRY CARTER
Department of Ch. E. & Materials Science, University of Minnesota, Minneapolis, MN 55455

N. RAVISHANKAR
Materials Research Center, Indian Institute of Science, Bangalore 560012, India

The sintering process of ceramics involves mass transport across grain boundaries resulting in the migration of these boundaries. When there is a liquid at the interface—as in liquid-phase sintering—the mass transport can be enhanced. In this study, electron backscatter diffraction has been used to examine grain-boundary migration of controlled interfaces in alumina. The interfaces were prepared by hot pressing single-crystal and polycrystalline alumina to single-crystal alumina substrates of known orientation. EBSD patterns, taken near the sintered interfaces, have been used to study the effects of crystallography on migration direction and rate.

1. Introduction

Grain boundary migration (GBM) in the presence of a liquid phase is an important phenomenon that occurs under a variety of mechanisms and processing conditions. One of the most common of these conditions is the densification process that occurs during liquid-phase sintering (LPS). The processes which occur during LPS have been studied extensively [1–22]. LPS is an important ceramic processing technique wherein ceramic powders and compacts are densified. One of the main advantages of LPS over solid-state sintering (SSS) for densification is the enhanced matter transport across the interface. For many solid powders, SSS is a very slow process that must be conducted at high temperatures. The addition of the right liquid phase to a solid powder can, in many cases, enhance the kinetics of sintering and thereby increase the rate of densification at a relatively low temperature [2, 23, 24]. Another advantage of LPS is the ability to tailor the microstructure and optimize material properties. There are many industrial and technological materials for which LPS is an integral part of the processing, leading to or enhancing the desired properties of the material. For example, silicon nitride alloys have shown improved fracture toughness as a result of LPS [25], and electronic devices made from barium titanate or zinc oxide are liquid-phase sintered not only to densify the material but also to enhance the desired electronic properties [26, 27]. Conversely, there are many applications for which the intergranular glass layer adversely affects the properties of the material. The GBM that occurs during LPS, in many instances, is the process that has the greatest effect on the materials properties [28]. In order to understand those effects, it is important to study the factors which affect the GBM.

In this study, single-crystal sapphire substrates and polycrystalline alumina have been used to study the effects of crystallography on the migration of grain boundaries in the presence of a liquid film. The film present at the interface is a glassy phase of anorthite ($CaAl_2Si_2O_8$), which forms a liquid during sintering. The solution and reprecipitation compositions of the alumina–anorthite system are equivalent at the sintering temperature, eliminating this as an influence on the driving force for GBM [29, 30]. The glass-containing interface is fabricated with an initially flat geometry. This allows for greater control over the original interface misorientation on the single-crystal side, and it minimizes the influence of curvature effects on the mass transport. Electron backscatter diffraction (EBSD) and electron imaging in the SEM were used to acquire orientation and misorientation data to complement grain size and grain shape measurements. These data were then analyzed to identify the existence, if any, of correlations between the GBM and the crystallography of the glass-containing interface and of the free surface near the interface.

0022-2461
DOI: 10.1007/s10853-006-6482-2

2. Background

Because of the close relationship between LPS and GBM, many of the concepts and theories developed for LPS are directly applicable to GBM. Therefore, a brief summary of LPS, as it relates to GBM, is presented here. In order to simplify the discussion, it is assumed that three requirements for LPS, as set forth by earlier studies [3, 5, 31, 32], have been fulfilled. Those requirements are: (i) a liquid film is present at the sintering temperature, (ii) there is good wetting of the grains of the solid by the liquid, and (iii) the solid is sufficiently soluble in the liquid. With these requirements satisfied, LPS can then be summarized into three main steps or stages. The first is the local rearrangement of the wetted solid particles, which proceeds toward reducing porosity while concurrently reducing surface free energy. The second stage is solution precipitation, which is described as dissolution of the solid at one surface and the precipitation of the solutes on another surface. The third stage is pore reduction or pore removal. Although the three stages successively dominate the densification process during LPS, there is obviously considerable overlapping between the stages [5, 19, 31]. GBM in the presence of a liquid phase is equivalent to grain growth in LPS, in the sense that in order for grain growth to occur, material from one grain must be moved to the surface of another. In other words one grain grows at the expense of another. There are several possible pathways by which grain growth may take place [33–35]. However, in the presence of a liquid film, and with regard to GBM, the predominant mechanism is solution/precipitation, wherein material from one solid surface is dissolved into the liquid phase and then are reprecipitated onto the solid surface across the interface [34]. This is also termed liquid-film migration (LFM) [10, 36–39].

In order for GBM to occur by the solution/precipitation mechanism, there must be adequate wetting of the solid surfaces by the liquid, sufficient solubility of the solid in the liquid, and finally, there must be a driving force, which causes a flux of solutes across or along the boundary. There are several factors that influence the driving force for mass transport [40]. For example, it is affected by a difference in the composition of the dissolved phase and that of the precipitated phase, the grain boundary shape, and the crystallography of the bounding planes at the interface. In different ways, each of these factors changes the chemical potential of the surface of the grain. The difference in chemical potential between two solid surfaces in the presence of a liquid phase can be simplified to a representation of the solubility of the solids in the liquid, or

$$\Delta\mu = (RT \ln c - RT \ln c_o) \tag{1}$$

where c represents the solubility of one surface and c_o the solubility of the other. This difference can be determined using the example of a spherical particle (solubility c) and a planar surface (solubility c_o). The work required to change the size of the spherical particle by the volume, Ω_m, of one mole of material is equal to a change in surface energy γdA. For the spherical particle Equation 2 becomes

$$RT \ln \frac{c}{c_o} = \gamma dA = \gamma 8\pi r^2 dr \tag{2}$$

and since the change in radius of a spherical particle is $dr = \Omega_m/4\pi r^2$, then the increase in solute concentration around the spherical particle is given by

$$c = c_o \exp\left[\frac{\gamma \Omega_m}{RT}\frac{2}{r}\right] \tag{3}$$

which is the Thompson–Freundlich equation for spherical particles [27, 41]. The equation for faceted particles is given by

$$c = c_o \exp\left[\frac{2\Omega_m}{3RT}\sum\left(\frac{a_i \gamma_i}{x_i}\right)\right] \tag{4}$$

where x_i is the distance of the ith facet from the particle center, a_i is a shape constant and γ_i is the specific liquid–solid interfacial energy of the ith facet. In the presence of a liquid film the surface-energy term must be replaced by liquid–solid interfacial energy, which would be specific to the different facets on the solid surface. Therefore, in cases where there is no difference between the solution and precipitation compositions and where there is an absence of curvature effects, the main influence for the driving force of GBM arises from the orientation of the bounding planes. As was shown above, the driving force for mass transport, F_t, is proportional to both the solid–liquid interfacial energy and the grain-boundary curvature or faceting, both of which are directly dependent on the orientation.

It has also been shown that the rate of GBM is highly dependent on the orientation of the bounding planes. The rate of GBM is determined by F_t, and the grain boundary mobility, M_{gb} [42, 43]:

$$V_{gb} = M_{gb} F_t \tag{5}$$

The grain boundary mobility is limited either by the transport of the solutes across the liquid film or by the rate of atom detachment or adsorption at the liquid–crystal interface. Therefore the rate of GBM in the presence of a liquid film can be controlled by either a diffusion-limited or reaction-limited mobility. The diffusion-limited mobility can be represented as:

$$M_{gb} = \frac{D_l c \Omega}{\delta kT} \text{(diffusion limited)} \tag{6}$$

where D_l is the diffusivity of the solute through the liquid, c is the solubility of the solid in the liquid, Ω is the volume of the solute in the liquid and δ is the film thickness. It has been shown that for low volume fractions of the liquid phase (<20%), the thickness of the film at the interface is dependent on the crystallography of the solid surfaces [44, 45]. High-energy boundaries have been found to be completely wetted by the film, whereas low-energy boundaries contained no film [30]. For higher volume fractions of liquid the film becomes continuous and the thickness depends on the volume fraction.

When the mobility of the boundary is limited by the rate of atom detachment or adsoption, it is considered reaction-limited and can be represented as:

$$M_{\mathrm{gb}} = \frac{K\Omega}{kT}(\text{reaction limited}) \tag{7}$$

where K is an interface reaction constant that depends on the density of dissolution/precipitation sites on the surface of the grain, which is directly related to the orientation of the surface and the temperature. K is also affected by the kinetics of the reaction and the driving force [43, 46].

Grain growth and GBM in Al_2O_3 have been studied extensively [13, 47]. Many studies have focused on the effects of impurities, including solutes, liquid phases or dopants, on the GBM of alumina [48–50]. A common experimental approach has been to introduce a large, single-crystal grain into a polycrystalline or fine-grained matrix [51, 52]. The amount of boundary migration over time at the single crystal is then used to determine the boundary mobility. It has been confirmed experimentally that a dependence of the growth kinetics on factors such as composition, temperature and crystallography have a broad influence on the grain-boundary mobility [18, 53]. For example, the growth rate of single-crystal sapphire into fine-grained Al_2O_3, in the presence of a glass phase, has been found to be orientation dependent with slower growth occurring in the ⟨0001⟩ direction, compared with other crystallographic directions. Even without the glass phase, the growth of single-crystal sapphire into polycrystalline Al_2O_3 was still found to be orientation dependent [18].

Another influence of the driving force for GBM is the wetting behavior of the glass at the interface. Studies conducted using anorthite liquid on free surfaces and interfaces of polycrystalline alumina have shown that there is a strong dependence of the wetting behavior on the crystallography of the surfaces [51, 54–59]. Of course, the wetting is also dependent on the availability of glass to the interface. Experimentally, the amount of liquid available to the interface can be controlled by depositing the glass film on the single-crystal substrate [21]. Once the glass becomes liquid, it is expected, although not intentional, that the liquid will also infiltrate adjacent boundaries in the polycrystalline material [60]. Therefore, it is expected that the amount of liquid present near the fabricated interface will decrease over time so that the wetting behavior, and therefore the migration rate, may be affected as a result.

The wetting behavior of the interface can also be affected by the presence of a free surface. Under certain conditions, it has been observed that the liquid phase migrates out of the boundary at the annealing temperature [29, 61, 62]. The exudation of the liquid can be mainly attributed to capillary forces, but is also affected by the surface energies of the adjacent free surfaces and the composition of the liquid, which may be altered near the free surface due to vaporization of the different components of the liquid [63]. Upon cooling, the liquid dewets and solidifies on the free surface [57, 64]. Depending on the rearrangement of the liquid within the boundary, the exudation and the compositional changes of the liquid near the surface, may cause a difference in the liquid–solid interactions occurring near the free surface, and those occurring deeper into the interface.

Other studies on free-surface effects on GBM have focused on grain-boundary grooving [65–68]. At high temperatures a groove can form at the intersection of the grain boundary and the free surface. The groove is formed either by evaporation or by diffusion of material on the surface or in the bulk, or by a combination of methods. The effect of the grain-boundary groove on the migration of the boundary has been studied in polycrystalline Cu [65]. It was shown that the groove can temporarily pin the interface at the surface. Evidence of this can be seen as remnant grooves on the surface that lie between the original location of the interface and the migrated location.

The formation of grain-boundary grooves and the wetting of the free surface by the liquid from the interface are made more significant to the mobility of the interface by the fact that the energies of the surfaces of alumina can differ by as much as 20% [69]. Therefore the change in energy caused by wetting a free surface by the liquid can be significant, as can the consumption of a high-energy surface by the migration of an interface. Many of the factors which can influence the chemical potential difference, driving the migration (Equation 2) in alumina can be directly associated with the surface energies of the crystallographic planes bounding the interface. The energies of specific low-energy planes in alumina have been calculated using atomistic lattice simulations [69–74]. The low-energy planes of alumina have also been verified experimentally by studying the faceting behavior of pores, interfaces and free surfaces [56–59, 75–77]. In the calculated models the low-energy planes have been shown to be the $c(0001)$, $r\{\bar{1}012\}$, $s\{1\bar{1}01\}$, $a\{11\bar{2}0\}$, $m\{10\bar{1}0\}$ and $p\{11\bar{2}3\}$. However, it has been shown experimentally that the prismatic $m\{10\bar{1}0\}$ plane, in air and in glass, is unstable at high temperatures and facets into the $s\{1\bar{1}01\}$ and the $r\{\bar{1}012\}$ planes [77, 78].

3. EBSD analysis

The relatively recent development of the use of automated EBSD detection systems enables the improved analytical study of oxides [79, 80]. A data map of the area is generated which contains for each data point: the Euler angles representing the orientation of the material, the band locations and pattern quality, and of course, the *x*-*y* coordinates of each data point. The orientations of the sample are most easily illustrated using an inverse pole figure (IPF) map. The quality of the EBSD patterns is also determined as the data are collected and can be used to create an image quality (IQ) map. The IQ map is created by measuring the quality (i.e., a measure of the contrast of the band edges) of the patterns and assigning a grayscale value—white representing the highest relative pattern quality and black the lowest. The IQ map is useful for locating grain boundaries and other areas where the pattern quality is low. The grain boundaries typically have a low pattern quality because either as the beam crosses the boundary the pattern becomes very weak, or there are two weak overlapping patterns from either side of the boundary: the boundary then appears as a dark line in the IQ map. Since the sample is tilted 70° about the *x*-axis (horizontal in the image) when the EBSD patterns are collected, the incremental step size used to collect the patterns is appropriately shortened in the *y* direction so that the desired step size is maintained with respect to the surface of the sample. Then the maps can be displayed as a tilt-corrected image of the surface.

4. Experimental

The samples used in this study were fabricated by joining polycrystalline alumina to single-crystal, glass-coated sapphire substrates by hot-pressing. First the polycrystalline and single-crystal material were polished flat, with the single-crystal sapphire polished parallel to either the (0001) plane or the $\{01\bar{1}0\}$ plane. A thin layer of anorthite glass (~100 nm) was then deposited on the polished surface of the single crystal using pulsed-laser deposition (PLD). The deposition was carried out at room temperature and 10 mTorr oxygen partial pressure using a laser energy of 200 mJ/pulse and a 10 Hz pulse repetition rate. The KrF ($\lambda = 248$ nm) excimer laser of the PLD system was focused onto a rotating target of anorthite glass, which was approximately 6 cm from the sapphire substrate surface. Greater detail on the technique of the film growth has been given in previous work [81]. The polished surfaces of the two materials were then hot pressed together at 1650°C for 30 min. A schematic of the sample geometry during the hot pressing is shown in Fig. 2a. The coupled structure was then polished perpendicular to the newly created interface using successively finer grades of diamond lapping films. The final polish was performed using a 0.05 μm diamond suspension on a padded polishing wheel. The final specimen geometry was such that the glass-containing interface was closely perpendicular to the polished free surface, approximately 1.5–2.0 mm in length and initially straight for each sample. A schematic of the polished sample geometry is shown in Fig. 2b.

TABLE I Summary of initial orientation of the samples fabricated for this study

	Orientation of single-crystal sapphire	
Samples	Interface	Free surface
c/poly (m)	*c*(0001)	$m\{10\bar{1}0\}$
c/poly (*a*)	*c*(0001)	$a\{11\bar{2}0\}$
m/poly	$m\{10\bar{1}0\}$	$a\{11\bar{2}0\}$

This sample design allowed for control of the initial crystallography on the single-crystal side of the interface in each of the samples, and it allowed for control of the composition of the interfacial glass. Therefore, the fabrication and heat treatment of the different samples was kept constant, but the orientation of the single-crystal side of the samples was changed. In samples where the bounding plane on the single-crystal side is the *c*(0001) plane, the sample is referred to as a *c*/poly sample, and where the bounding plane on the single-crystal side is the $m\{01\bar{1}0\}$ plane, the sample is referred to as an *m*/poly sample. Two different types of *c*/poly samples were fabricated and analyzed: *c*/poly (*m*) was fabricated with the $m\{01\bar{1}0\}$ plane parallel to the free surface and *c*/poly (a) was fabricated with the $a\{11\bar{2}0\}$ plane parallel to the free surface. Only one type of *m*/poly sample was fabricated with the $a\{11\bar{2}0\}$ plane parallel to the free surface. A summary of the samples and their initial orientations is shown in Table I.

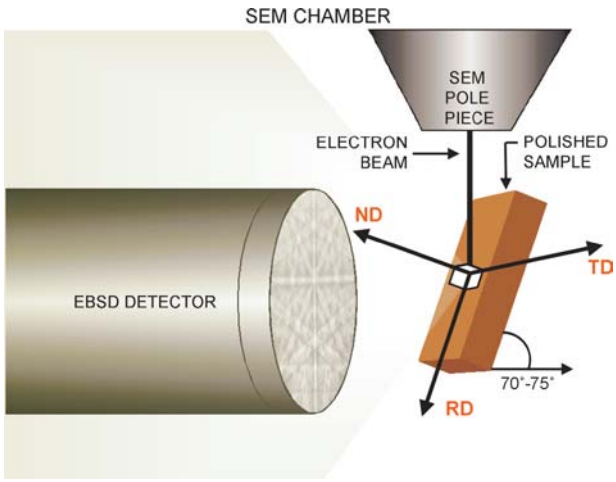

Figure 1 A simplified schematic of the EBSD automated detection system. The system is attached to the SEM chamber and consists of a phosphor screen placed near a highly tilted (~70°) specimen. The patterns appearing on the phosphor are imaged using a CCD camera and then analyzed by computer. The axes shown on the surface of the sample act as a reference to the orientations acquired by the system. The axis system is labeled "ND" (normal direction or 001), "RD" (reference direction or 100) and "TD" (transverse direction or 010).

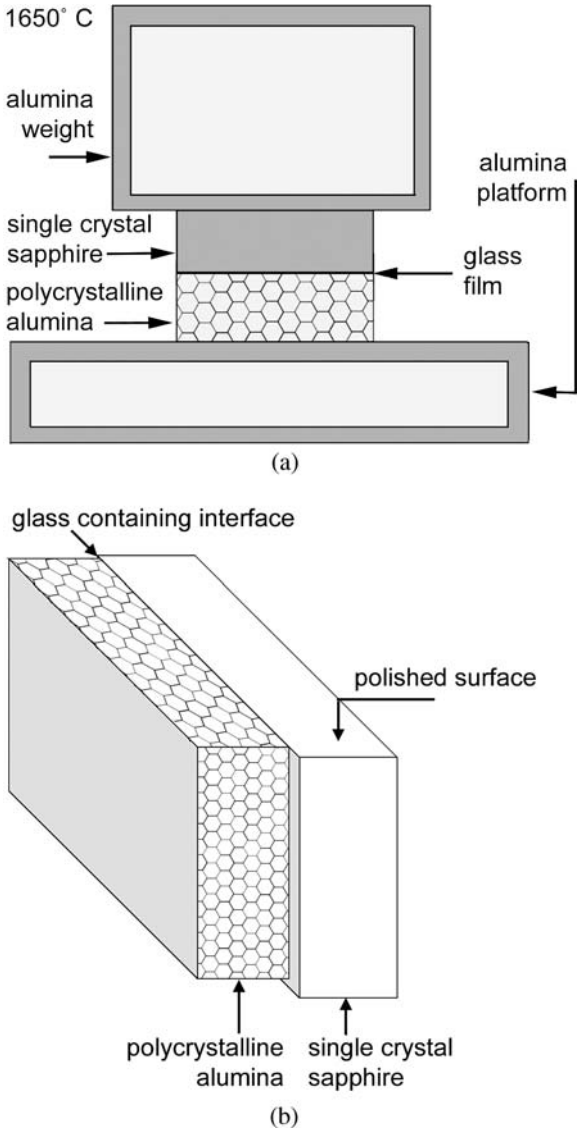

Figure 2 (a) Schematic of the experimental geometry used during fabrication of the glass-containing interface. (b) Schematic of the sample geometry after polishing the surface perpendicular to the glass-containing interface.

All of the samples were annealed for 20 h at 1650°C and characterized by visible-light microscopy (VLM), scanning electron microscopy (SEM) and electron backscatter diffraction (EBSD). This first characterization was performed on what will be referred to as the "as-annealed surface," which is the surface that was polished prior to the anneal treatment. No further processing was carried out on this surface between the anneal treatment and the first characterization except for the deposition of 1–2 nm of Pt to reduce charging in the SEM. The free surface was then ground to remove approximately 400 μm of material and polished in the manner described above, parallel to the original cross-section surface. After the deposition of the conductive coating, a second characterization, similar to the first, was performed on what will be referred to as the "polished surface."

Secondary electron (SE) imaging was performed using a field-emission scanning electron microscope (FESEM) operating at 5 kV. Single EBSD patterns were acquired and indexed using a custom-designed EBSD interface system that was installed on a LaB_6 SEM [82, 83]. Orientation maps, pole figures and grain-size measurements were performed using a commercially designed EBSD/OIM system installed on a FESEM [84]. SEM samples were coated with 1–2 nm of Pt to minimize charging in the SEM.

In order to study the interface just below the surface, a transmission electron microscope (TEM) cross-section sample was prepared using the focused-ion beam (FIB) technique. The cross section was prepared from an alumina bicrystal in order to control the orientation of both sides of the interface. The bicrystal was fabricated by hot-pressing coated, single-crystal $c(0001)$-plane substrates of sapphire to clean $m(01\bar{1}0)$-plane single crystals; the thin films (~100 nm of anorthite glass) were deposited using the pulsed-laser deposition (PLD) process. The bicrystal was polished to yield a smooth surface perpendicular to the grain boundary and annealed at 1650°C for 2 h. The cross section of the interface was prepared to include the free surface at the edge of the TEM sample. Images and diffraction patterns of the sample were acquired using a Philips CM30 TEM operating at 300 kV.

5. Results

After the final anneal treatment, all of the samples exhibited an interface line that had migrated from its original position. In order to observe and measure the migration at the free surface, the original location of the interface had to be determined. For the as-annealed surface, this was accomplished by observing, in the SEM, the surface grooves left behind by the migrating interface. Fig. 3 is an SEM image of the surface of one of the *c*/poly samples that shows the remnant surface grooves. The image in Fig. 3 was acquired with the sample tilted to 70°. It was found that the remnant surface grooves were more readily observed if the sample was tilted with respect to the electron beam. In this case, the sample was also tilted in preparation for the acquisition of EBSD patterns. The extent of the migration was then measured from the remnant groove to the new location of the migrated boundary.

For the polished surface, the original location of the interface was found by acquiring an image of the entire interface by VLM or low-magnification SEM. Then a line was drawn connecting the two sides of the migration couple where the single-crystal substrate is overhanging the polycrystalline material. This method is illustrated in the schematic shown in Fig. 4. The line locating the original interface is shown on the schematic as a dotted line. Measurements of the migration distance were then made from this line to the migrated boundary location. In order to confirm the validity of this method, the GBM at

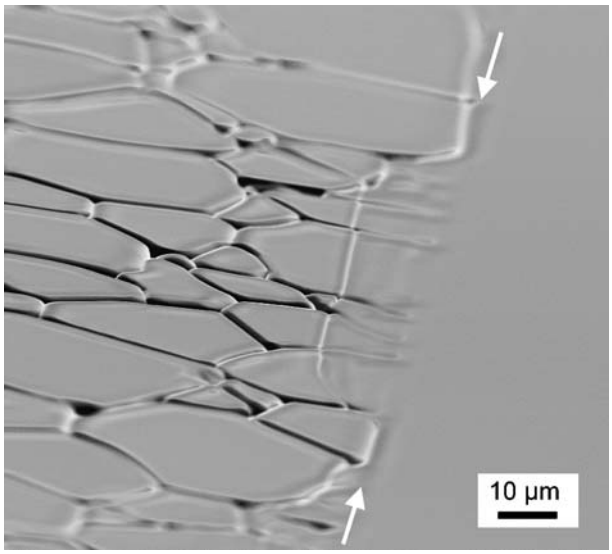

Figure 3 SEM image of a portion of the as-annealed surface of *c*/poly (a). The image was acquired with the sample tilted to 70° which facilitated the observation of the remnant surface grooves left behind by the migrating interface. A portion of the interface (between the arrows) had migrated into the polycrystalline alumina as much as 12 μm. The arrows indicate the original location of the interface determined by the locations of the remnant grooves.

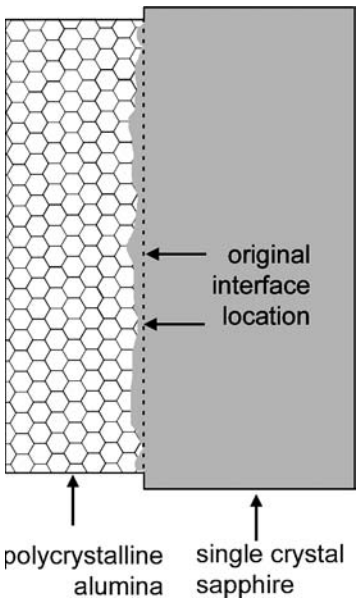

Figure 4 Schematic of the as-annealed surface of the sample illustrating the method for determining the initial location of the glass-containing interface.

the free surface was also measured by this method and the measurements were found to be consistent using either method for locating the original interface.

The glass-containing interface in all of the samples was found to move into the polycrystalline side of the sample such that grains on the polycrystalline side, that border the initial interface, were partially or wholly consumed by the single-crystal substrate. However, differences were found

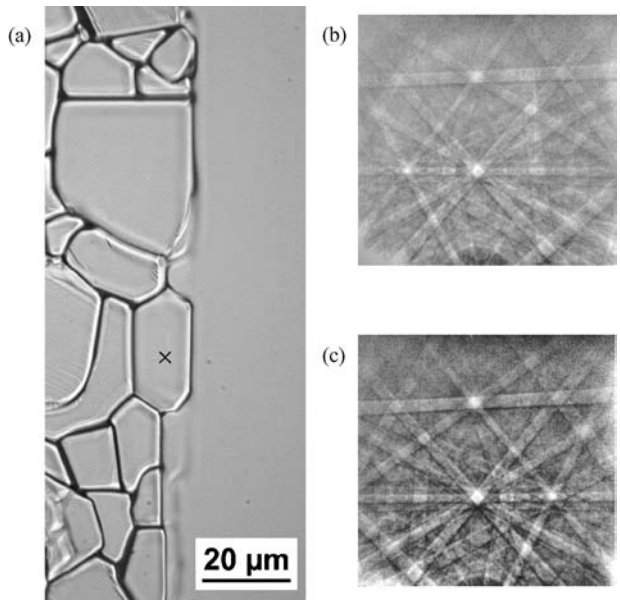

Figure 5 (a) VLM image of the interface between the single-crystal and polycrystalline alumina. Several grains have pinned the interface at its original location. (b) EBSD patterns of the grain marked with an "X", and (c) the single-crystal side of the interface reveal that the orientation relationship is that of a "special" grain boundary.

in the amount and uniformity of the migration from sample to sample. In samples *c*/poly (*m*) and (a), large sections of the interface line had migrated as much as 12 μm into the polycrystalline material. This can be seen clearly in the SEM image in Fig. 3. There are also grains bordering the interfaces of these two samples at which there appears to have been little or no migration. A few such grains are shown in the VLM image in Fig. 5 which is a higher magnification image of a part of the interface in sample *c*/poly (b). Individual EBSD patterns acquired from the grains bounding the interface and the single-crystal substrate were used to determine the orientations and misorientations. The patterns showed that a few grains had a special misorientation with the substrate. The grain labeled with "X" shown in the VLM image in Fig. 5a was found to have a special (presumably low-energy) grain boundary at the interface. Indexing of the EBSD patterns indicated an alignment of the prismatic planes of the grain and the single crystal. The misorientation angle was determined to be approximately 180° about a $[01\bar{1}0]$-type axis (a near-$\Sigma = 3$ grain boundary). Assuming the interface bounding planes are still perpendicular to the free surface, then both sides of the interface would be the (0001) plane. The EBSD patterns acquired from the grain and the sapphire substrate are shown in Figs. 5b and c.

In the *c*/poly samples, it was found that the majority of the boundary trace remained parallel to its original direction. Therefore the interface line between the grains on the polycrystalline side and the single crystal remained flat and parallel to a direction on the basal or (0001) plane of the single-crystal sapphire.

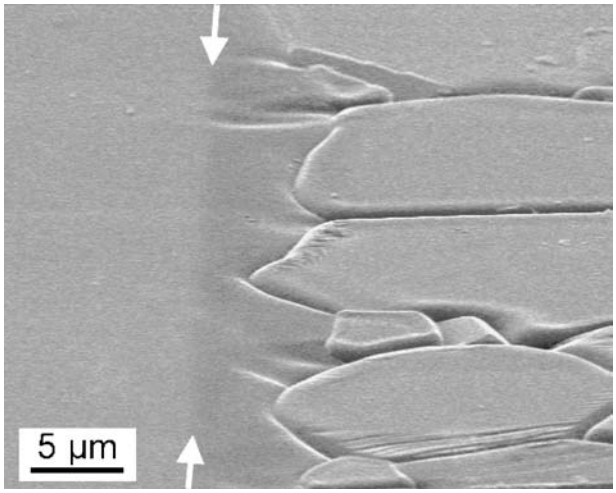

Figure 6 SEM image of a representative portion of the glass-containing interface of the *m*/poly sample which shows rounding of the grains at the interface. The image was acquired with the sample titled 70° to the electron beam to give contrast to the original location of the interface (indicated by the arrows).

The migration behavior of the interface in the *m*/poly sample was different from that of the *c*/poly samples. In this sample, it was found that the amount of migration across the sample was also very non-uniform, but the boundary trace did not remain parallel to its original direction. The grains bordering the main interface appeared more rounded on the interface side, so that the boundary traces are no longer parallel to a direction on the basal plane of the single-crystal sapphire. Fig. 6 is an SEM image of a representative portion of the main interface in the m/poly sample, which shows how the grains have become more rounded and a greater amount of migration has occurred at the triple junctions. The image in Fig. 6 was acquired with the sample tilted 70° to give contrast to the migrated region and in preparation for EBSD pattern collection.

The amount of migration at each grain in the *c*/poly samples was determined by measuring the distance from the location of the original interface line to the migrated line at the midsection of the grain. Since the migrated boundary traces were, for the most part, parallel to the direction of the original boundary traces, this method of measurement yielded an average migration distance for each sample, that weights the grains equally, independent of boundary-trace length. The standard deviation was used to determine the "uniformity" of the migration. This same method was used to obtain only the standard deviation of

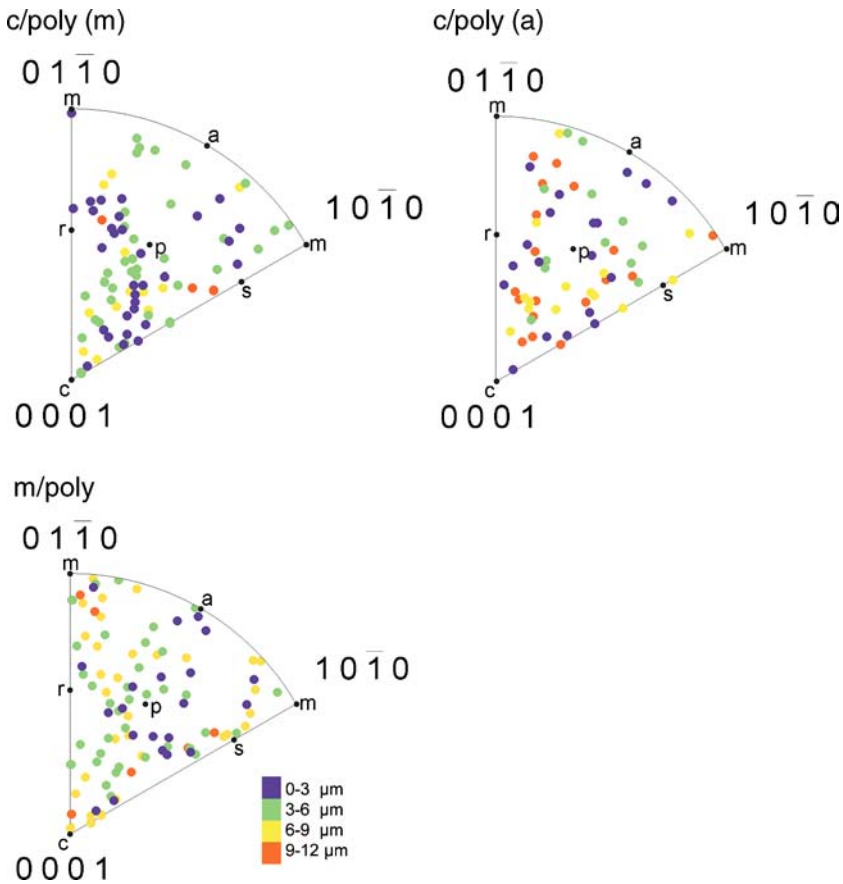

Figure 7 Inverse pole figures of the free surface of samples *c*/poly (m), *c*/poly (a), and *m*/poly. For each grain bordering the interface, the crystallographic planes parallel to the free surface are plotted, one point per grain, on the inverse pole figures and colored according to the corresponding amount of migration at the grain.

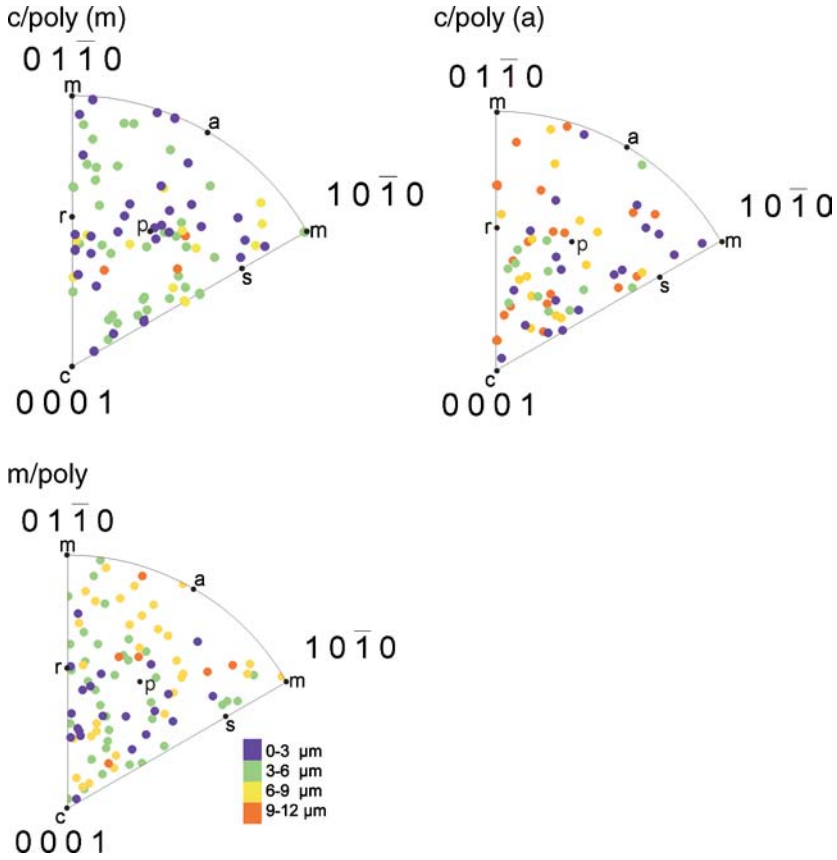

Figure 8 Inverse pole figures of the interface bounding planes of samples *c*/poly (m), *c*/poly (a), and *m*/poly. For each grain bordering the interface, the crystallographic planes parallel to the interface are plotted, one point per grain, on the inverse pole figures and colored according to the corresponding amount of migration.

the migration for the *m*/poly sample. The average migration in the *m*/poly sample was measured by imaging the entire interface and using graphics software to measure the area between the original location of the interface and the migrated location. The area was then divided by the length of the original interface to yield an average migration distance that included the migration at the triple junctions. The average migration distance for each of the samples is shown in Table II.

The uniformity of migration, shown in Table II, is simply a number derived from the average migration, μ, and the standard deviation of the average migration, σ. The equation for the uniformity is then:

$$1 - \frac{\sigma}{\mu} \tag{8}$$

The calculation of this (average) uniformity is meant only as a comparison between samples and between the different analyses performed. The uniformity of migration of the two *c*/poly samples was very similar at the free surface. The *m*/poly sample was slightly more uniform than the *c*/poly samples.

The entire interface length was scanned with the EBSD detector, which allowed for the correlation between GBM amount and crystallography at the interface. More specifically, the migration distance at each grain on the polycrystalline side of the interface was correlated with the orientation of the free surface of the grain. These data are combined for each sample and shown in Fig. 7. In this figure the crystallographic planes parallel to the free surface are plotted, one point per grain, on inverse pole figure (IPF) plots and colored according to the corresponding migration distance. The migration distance of each grain was then compared to the orientation of the grain's interface bounding plane. This comparison is also shown by IPF plots (Fig. 8). The plots in both Figs 7 and 8 also indicate alumina planes which have been shown to

TABLE II Summary of average migration distances and description of migration behavior at the as-annealed surface of all samples

Samples	Average migration distance (μm)	Uniformity of migration	Interface line
c/poly (*a*)	6.1	0.36	flat and parallel to *c*-plane
c/poly (*m*)	3.7	0.38	flat and parallel to *c*-plane
m/poly	5.3	0.47	grains rounded at interface

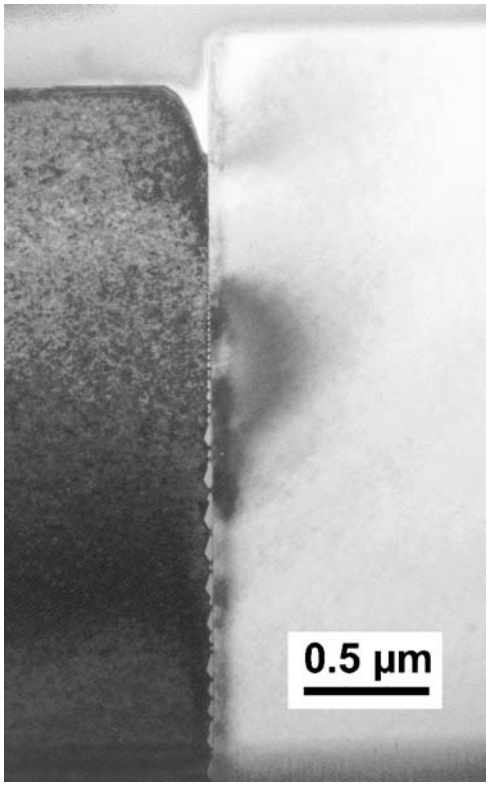

Figure 9 A bright-field TEM image of the FIB-prepared cross section. The boundary had moved from right to left approximately 3 μm.

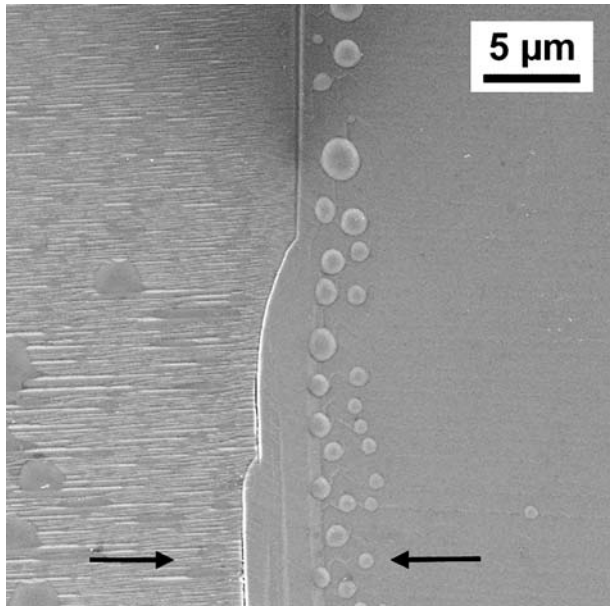

Figure 10 A secondary-electron SEM image of an alumina bicrystal. The boundary in the lower half of the image has migrated approximately 3 μm to the left. The arrows indicate from where in the bicrystal the cross-section sample was prepared.

be stable at high temperatures and the *m* plane which is known to be unstable at high temperatures [58, 75, 76]. An examination of the IPF for the free surface of sample *c*/poly (*m*) reveals that there is a definite clustering of orientations between the *r* and *p* planes and also between the *p* and *c* planes. These points are significant because they represent the grains which showed the lowest migration distance occurred (0–3 μm). The IPF of the free surface of the *m*-poly sample appears to have only a slight clustering of the low-migration orientations around the *p* plane and *a* planes. The IPF of the free surface of *c*/poly (a) appears to be far more random than the other two.

For the measurements shown in Fig. 8, it was assumed that the inclination of the interface is perpendicular to the free surface. This assumption is based on transmission electron microscopy (TEM) studies of alumina interfaces which contain anorthite glass. TEM cross sections that have been prepared of interfaces which have migrated, have shown that if one of the bounding planes is the *c*(0001) plane, the boundary will remain parallel to the *c*-plane side of the interface [53]. Fig. 9 is a bright-field (BF) image of a FIB-prepared TEM cross section of the migrated interface of an alumina bicrystal. The interface is vertical in the image with the direction of migration being from right to left. Fig. 10 shows an SEM image of the free surface of the bicrystal prior to cross sectioning, which reveals that the interface had migrated approximately 3 μm to the left. The top of the sample shown in Fig. 9 is part of the original surface shown in Fig. 10 (between the arrows). Electron diffraction analysis of the two sides confirmed that the bounding planes on the right and left sides of the interface are the *c*(0001) and *m*$(01\bar{1}0)$ planes respectively. The interface has remained parallel to the *c*-plane which appears flat in the image. The *m*-plane, however, has faceted with the facets decreasing in size and frequency the closer they are to the original surface of the bicrystal.

Greater detail of the interface can be seen in Fig. 11, which is another BF image of the interface taken at higher magnification. The selected-area diffraction pattern is shown in the inset. The left side of the bicrystal is oriented to the $[2\bar{1}\bar{1}0]$ zone axis and the facet planes are viewed edge–on. The interface plane on the left is actually facetted parallel to the $(01\bar{1}1)$ and $(0\bar{1}12)$ planes [77].

The as-annealed surface of each of the polycrystalline samples was then polished down >400 μm in order to analyze the migration behavior in the bulk. Initially the only difference between the two *c*/poly samples was the orientation of the free surface. At the polished surface however, this difference becomes insignificant and the behavior and amount of migration become very similar. Therefore, the data from the *c*/poly samples is combined in this section.

The flat polished surface gave very little contrast using either secondary-electron imaging in the SEM or VLM. Therefore, the polished surface of the samples was "imaged" using the EBSD data. IPF maps and image quality (IQ) maps were used to determine the migration

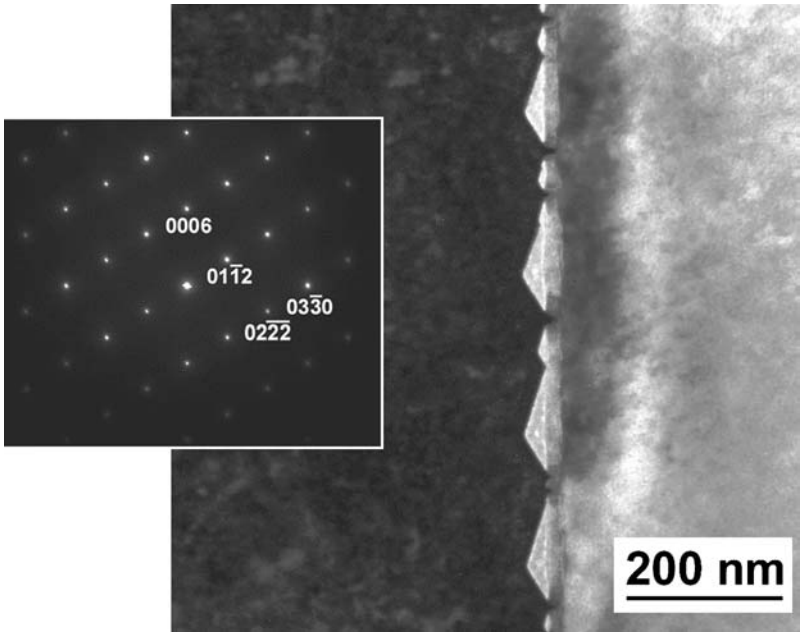

Figure 11 A bright-field TEM image of part of the interface recorded at higher magnification. The selected-area diffraction pattern of the left grain is shown in the inset. The bicrystal is oriented such that the facet planes are viewed edge-on.

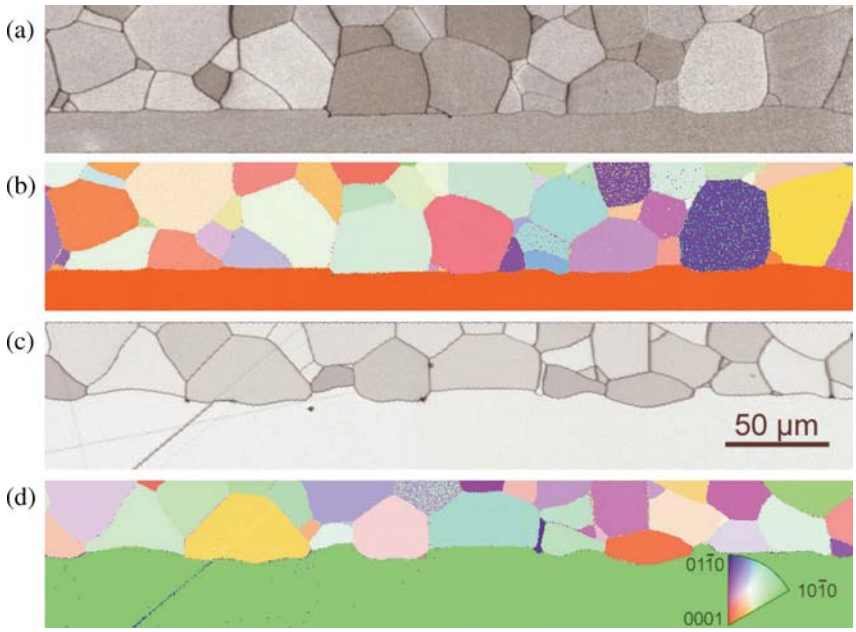

Figure 12 IQ maps and IPF maps of representative regions of a *c*/poly sample (a) and (b) and the *m*/poly sample (c) and (d). The grain boundaries appear as dark lines in the IQ maps. The IPF map is a color representation of the crystallographic directions perpendicular to the interface.

distance and the shape of the interface line. Fig. 12 shows IPF and IQ maps of representative regions from a *c*/poly sample and the *m*/poly sample. Similar to that of the as-annealed surface, the interface line of the *c*/poly samples remained parallel to the original direction of the interface line at most of the grains along the interface. The migration appears to be more uniform along the length of the interface with fewer grains that have pinned the interface at its original location. The average migration of the *c*/poly samples was found to be very similar and is shown in Table III. The interface line at the polished surface of the *m*/poly sample, similar to that of the as-annealed surface, was found to be curved about the grains, with a greater amount of migration occurring at the triple junctions. The average migration amount, also shown in Table III, was found to exceed the migration at the as-annealed surface. The *m*/poly sample was slightly more uniform than the *c*/poly samples in both analyses,

TABLE III Summary of average migration and description of migration behavior at the polished surface of all samples

Samples	Average Migration (μm)	Uniformity of migration	Interface Line
c/poly (*a*)	5.8	0.42	flat and parallel to *c*-plane
c/poly (*m*)	5.9	0.53	flat and parallel to *c*-plane
m/poly	6.4	0.54	grains rounded at interface

with an increase in uniformity in the bulk analysis. The difference in uniformity between the *m*/poly and *c*/poly samples is attributed to the fact that there were fewer grains in the *m*/poly sample that pinned the interface.

The EBSD data were also used to compare the migration distance of each grain to the orientation of the boundary planes. For this measurement it is again assumed that the inclination of the interface is perpendicular to the free surface. This comparison is shown by the IPF plots in Fig. 13. In this figure the crystallographic planes parallel to the free surface (one point per grain), are plotted on IPFs and colored according to the migration distance at that grain. The plots in Fig. 13 also indicate the alumina planes that are stable at high temperatures and the *m* plane, which is known to be unstable at high temperatures. The IPF data for the *c*/poly samples are combined into one plot. A third plot is shown in Fig. 13, which was created from a polished surface of the same polycrystalline alumina material that was used to fabricate all of the samples. This plot is shown for comparison and represents a random distribution of over 500 alumina grains. The IPF plots of both the *c*/poly and *m*/poly data appear to have a fairly random distribution of low- and high-migration orientations.

6. Discussion

A comparison of the migration behavior of the samples at the free surface to that in the bulk revealed that two of the three samples yielded very different results. One of those, the *c*/poly (m) sample, was found to have a smaller average migration at the free surface than in the bulk. Table I indicates that the free surface of the single-crystal sapphire is parallel to the $m\{10\bar{1}0\}$ plane. The *m* plane of alumina is known to be unstable at high temperatures and facets into the $s\{1\bar{1}01\}$ and the $r\{\bar{1}012\}$ planes resulting

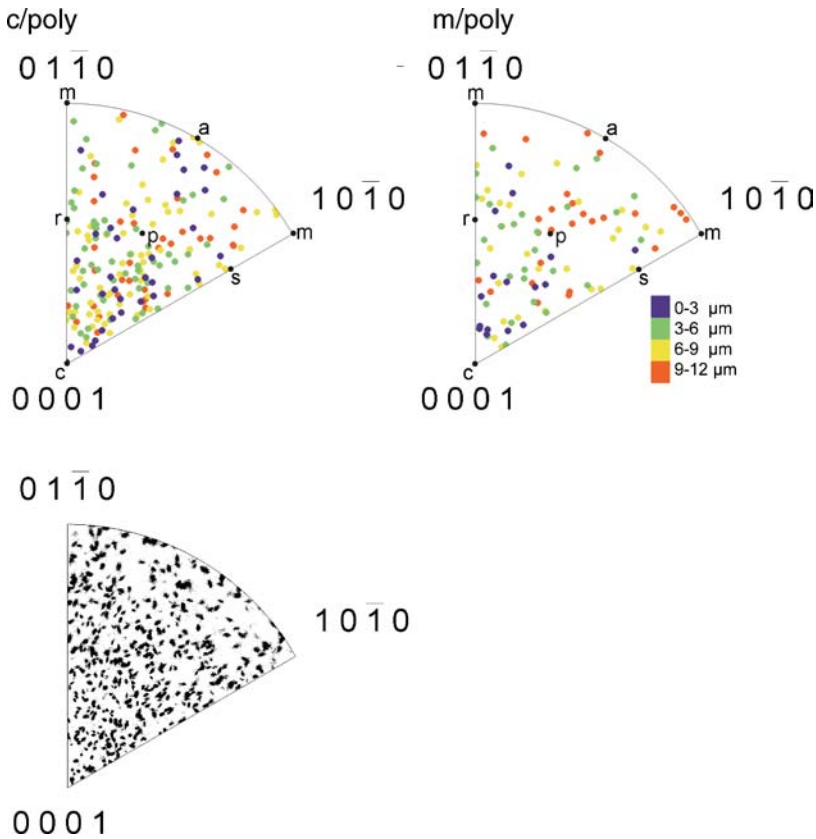

Figure 13 Inverse pole figures of the interface bounding planes of samples *c*/poly and *m*/poly. For each grain bordering the interface, the crystallographic planes parallel to the interface are plotted, one point per grain, on the inverse pole figures and colored according to the corresponding amount of migration. Shown for comparison, the third pole figure displays the orientation distribution from a random surface of the same polycrystalline alumina as that used for the migration samples.

in an approximate 10% increase in surface area. Taking this into account, the migration of the boundary at the surface may create a locally unfavorable condition by requiring the creation of a high-energy surface. Of course, the consumption of interfaces on the polycrystalline side of the sample could compensate for the energy created by expanding the faceted surface. However, if the liquid has exited the interface in order to wet the free surface of the sapphire, the mobility of the interface near the surface may be reduced by a lack of a transport medium.

The polycrystalline side of the interface, of course, creates a complication because of the large amount of interface that can be consumed by even a small amount of migration of the main interface thereby lowering the total energy. Therefore, the migration rate in the bulk could continue to exceed the rate at the surface and still move toward a lower energy configuration. Studies of GBM in alumina bicrystals, where two single crystals abut the interface, have shown remnant boundary grooves at the surface. The grooves indicate a temporary delay of the boundary mobility, but in this configuration the interface at the surface must maintain a migration rate that does not allow for the creation of an energetically unfavorable amount of interface [21].

The *m*/poly sample also showed a small difference between the migration amount at the free surface and that in the bulk. The *m*/poly sample is bounded on the free surface by the $a\{11\bar{2}0\}$ plane. Therefore, the probability that the liquid has exuded the boundary to wet the surface is less for the *m*/poly sample, since the energy of the free surface is lower than the surface energy of the bounding plane in the interface. The *c*/poly (a) sample is also bounded by the *a* plane on the free surface, but showed very little difference in migration amount. It is unclear why the *m*/poly sample exhibited a difference in migration where the *c*/poly (a) sample did not.

The shape of the interface line remained very similar in shape when comparing the migration at the surface of a sample to that in the bulk. However there was a difference in the interface line shape between the samples. It is apparent from the interface line shape (Fig. 12) that the *m* plane of alumina is less stable than the *c* plane. This is also evident from the TEM cross section shown in Fig. 9.

The TEM cross-section sample illustrates several aspects of this experiment. The bounding planes of the interface are the *m* and *c* planes. The *m* plane has faceted, but the facets coarsen as they get further from the free surface. It has been shown that, at high temperatures, the faceting behavior of alumina changes in contact with anorthite liquid [55]. The change in size of the faceting indicates a possible change in the amount of liquid available and/or a change in the interactions between the surface and the glass. It is possible that the thickness of the glass layer near the surface was decreased or completely eliminated due to exudation of the glass to wet the free surface [57].

The inverse pole figures of the planes parallel to the free surface (Fig. 7) show the comparison between the crystallographic plane parallel to the free surface and the corresponding amount of migration for each grain bordering the interface. The most significant of these pole figures are those created from the samples that have shown the greatest difference in migration behavior between the free surface and the bulk, or the *c*/poly (m) and the *m*/poly samples. The observation of low-migration points located on or near planes that are known to be stable at high temperatures is very significant in terms of the competing surface energies of the two sides of the interface. The *c*/poly (m) sample has a high-energy free surface on the single-crystal side of the interface. Therefore, a low-energy free surface on a grain of the polycrystalline material may have impeded the migration. On the free-surface IPF of *c*/poly (*m*) there are clusters of low-migration orientations between the *r* and *p* planes and the *c* and *p* planes. It has been shown that, at high temperatures, the surfaces of alumina will be faceted, and that the facets coincide with planes that are known to be stable [30, 55, 77, 85, 86]. The cluster of low-migration orientations between the *r* and *p* planes could very well be faceted parallel to these two planes. Since the angle between the *r* and *p* planes is only 26°, the increase in surface area would no more than 2.6%. The cluster of low-migration orientations that appear between the *c* and *p* planes would not be as low in energy since the angle between the *c* and *p* planes is 61.2°. For a surface orientation that lies directly between the *c* and *p* planes, the increase in surface area could be as much as 16%. Presently no experimental data exist that indicates whether another stable surface exists between the *c* and *p* planes. However, even with a 16% increase in surface area the surface may be lower in energy than that of the *m* plane.

The IPF of the surface orientations of the m/poly sample shows a weak cluster of low-migration orientations around the *a* and *p* planes. These orientations could also be accommodated by faceting parallel to the low-energy planes, but it is clear from the figure that more data are needed to establish a clear relationship between the surface orientations and the migration amount.

The first set of IPF plots of the planes parallel to the interface (Fig. 8), were also created from the data acquired at the free surface, and were prepared to test for a relationship between the low-migration orientations and the high-temperature stable planes. The existence of a relationship in these plots would weaken the argument that the energy of the free surface has an effect on the interface mobility. The low-migration orientations of the *m*/poly and *c*/poly (a) plots appear randomly distributed. The *c*/poly (m) plot, however appears to have a small cluster of low-migration orientations about the *p* planes. This could mean, of course, that the interface bounding plane is determining the mobility of the interface and not the free surface.

The IPF plots created from the data acquired at the polished surface (Fig. 13) do not show a clear relationship with the migration amount. In fact, when compared to the IPF created from a random distribution of orientations, the two plots from the samples appear to have a random distribution of orientations as well. This was an unexpected result considering that the migration amount has been shown to depend quite strongly on the crystallographic orientations of the bounding planes on the single-crystal side of the interface, or where both sides of the interface are single crystals, as in bicrystal studies [21, 53].

7. Conclusion

Glass-containing interfaces between single-crystal, $c(0001)$ plane and $m\{10\bar{1}0\}$ plane sapphire and polycrystalline alumina (Lucalox^{TM}) were annealed at 1650°C for 20 h and studied using a combination of SEM and VLM imaging and EBSD. The effects of different crystallographic orientations on the migration at the free surface were compared to that in the bulk. The *c*/poly (*m*) sample was found to have an average migration at the free surface which was much smaller than that found in the bulk. The *c*/poly (a) sample had an average migration similar to that found in the bulk and the m/poly sample had only a slightly smaller average migration at the free surface. The interface line in the *c*/poly samples remained mostly parallel to the original direction of the interface, although the migration amount varied from grain to grain. The interface line of the *m*/poly sample became curved with slightly more migration occurring at the triple junctions.

The *c*/poly (*m*) sample was the only sample to show a strong relationship between the crystallography of the free surface and the migration. It was found that the grains adjacent to low migration were oriented such that the planes parallel to the free surface were close to the *r* and *p* planes. It is proposed that the difference in the free-surface energies on either side of the interface may have an effect on the migration rate. TEM observations of a cross section of a migrated, glass-containing interface suggest that the amount of interfacial glass near the free surface may change during the anneal treatment, which could then affect the migration rate.

The preliminary work also suggests that there is no obvious relationship between the orientation of the bounding planes on the polycrystalline side of the interface and the migration amount.

Acknowledgements

The authors acknowledge many useful discussions with Dr. Shelley Gilliss and Ms. Nicole Munoz. They thank Chris Frethem for technical assistance with the Hitachi S-900 SEM. This research was supported by DOE under grant number DE-FG02-01ER45883.

References

1. J. W. CAHN and R. B. HEADY, *J. Am. Ceram. Soc.* **53** (1970) 406.
2. G. H. S. PRICE, C. J. SMITHELLS and S. V. WILLIAMS, *J. Inst. Metals* **62** (1938) 239.
3. F. V. LENEL, *Trans. AIME* **175** (1948) 878.
4. G. C. KUCZYNSKI, *ibid.* **185** (1949) 169.
5. W. D. KINGERY, *J. Appl. Phys.* **30** (1959) 301.
6. *Idem.* in "Kinetics of High-Temperature Processes" edited by K. D. Kingery, (Wiley, 1959) p. 187.
7. R. B. HEADY and J. W. CAHN, *Metall. Trans.* **1** (1970) 185.
8. W. J. HUPPMANN, H. RIEGGER, W. A. KAYSSER, V. SMOLEJ and S. PEJOVNIK, *Z.r Metall.* **70** (1979) 707.
9. R. M. GERMAN, "Liquid Phase Sintering" (Plenum Press, 1985).
10. J. E. MARION, C. H. HSUEH and A. G. EVANS, *J. Am. Ceram. Soc.* **70** (1987) 708.
11. R. RAJ and C. K. CHYUNG, *Acta Metall.* **29** (1980) 159.
12. G. M. PHARR and M. F. ASHBY, *ibid.* **31** (1983) 129.
13. R. L. COBLE and J. E. BURKE. in "Progress in Ceramic Science" edited by J. E. Burke, (Pergamon, 1963) vol. 3, p. 197.
14. V. N. EREMENKO, Y. V. NAIDICH and I. A. LAVRINKO, "Liquid Phase Sintering", (Consultant Bureau, 1970).
15. Z. S. NIKOLIC, *J. Mater. Sci.* **4** (1999) 783.
16. T. M. SHAW, *J. Am. Ceram. Soc.* **69** (1986) 27.
17. W. J. HUPPMANN and H. RIEGGER, *Acta Metall.* **23** (1975) 965.
18. W. A. KAYSSER, M. SPRISSLER, C. A. HANDWERKER and J. E. BLENDELL, *J. Am. Ceram. Soc.* **70** (1987) 339.
19. O.-H. KWON and G. L. MESSING, *Acta Metall. Mater.* **39** (1991) 2059.
20. Y. M. KOUH, C. B. CARTER, K. J. MORRISSEY, P. ANGELINI and J. BENTLEY, *J. Mater. Sci.* **21** (1986) 2689.
21. N. RAVISHANKAR and C. B. CARTER, *Acta Mater.* **49** (2001) 1963.
22. W. A. KAYSSER, in "Processing and Properties for Powder Metallurgy Composites," The Metallurgical Society/AIME, Denver (Colorado, USA, 1988) p. 21.
23. W. D. KINGERY, H. K. BOWEN and D. R. UHLMANN. in "Wiley Series on the Science and Technology of Materials" 2nd ed., edited by E. Burke, B. Chalmers and J. A. Krumhansl, (Wiley-Interscience, 1976) p. 425.
24. D. W. BUDWORTH, "An Introduction to Ceramic Science" (Pergamon Press, 1970).
25. M. K. CINIBULK, H.-J. KLEEBE, G. A. SCHNEIDER and M. RUHLE, *J. Am. Ceram. Soc.* **76** (1993) 2801.
26. M. MATSOUKA, *Japan. J. Appl. Phys.* **10** (1971) 736.
27. Y.-M. CHIANG, D. P. B. III and W. D. KINGERY. "Physical Ceramics" (John Wiley & Sons, 1997).
28. A. PAWLOWSKI, M. M. BUCKO and Z. PEDZICH, *Mater. Res. Bull.* **37** (2002) 425.
29. N. RAVISHANKAR and C. B. CARTER, *J. Am. Ceram. Soc.* **84** (2001) 859.
30. D. W. SUSNITZKY and C. B. CARTER, *ibid.* **73** (1990) 2485.
31. W. D. KINGERY and M. D. NARASIMHAN, *J. Appl. Phys.* **30** (1959) 307.
32. J. GURLAND and J. T. NORTON, *Trans. Am. Inst. Mining Metall. Eng.* **194** (1952) 1051.
33. W. A. KAYSSER, S. TAKAJO and G. PETZOW, *Acta Metall.* **32** (1984) 115.
34. W. J. HUPPMANN, *Z. Metall.* **70** (1979) 792.
35. L. KOZMA and W. J. HUPPMANN, *Int. J. Powder Metall.* **15** (1979) 115.
36. C. A. HANDWERKER, J. W. CAHN, D. N. YOON and J. E. BLENDELL, in "Diffusion in Solids: Recent Developments," The Metallurgical Society, Inc, Detroit, Michigan, USA (1985), p. 275.
37. Y.-K. PAEK, H.-Y. LEE and S.-J. L. KANG, *J. Am. Ceram.*

Soc. **79** (1996) 3029.
38. S. W. BARKER and G. R. PURDY, *Acta Mater.* **46** (1998) 511.
39. Y. BRECHET and G. R. PURDY, *Scripta Metall.* **22** (1988) 1629.
40. A. P. SUTTON and R. W. BALLUFFI, "Interfaces in Crystalline Materials," (Clarendon Press, 1995).
41. H. FREUNDLICH, Kapillarchemie, (Akad. Verlages, 1922).
42. J. D. POWERS and A. M. GLAESER, *Inter. Sci.* **6** (1998) 23.
43. H. GLEITER, *Acta Metall.* **17** (1969) 853.
44. D. R. CLARKE, *Ann. Rev. Mater. Sci.* **17** (1987) 57.
45. *Idem*., in "Surfaces and Interfaces of Ceramic Materials," edited by L.-C. Dufour, C. Monty and G. Petot-Ervas (Kluwer Academic Publishers, 1989) p. 57.
46. K. W. LAY, *J. Am. Ceram. Soc.* **51** (1968) 373.
47. R. L. COBLE, *ibid.* **41** (1958) 55.
48. R. D. MONAHAN and J. W. HALLORAN, *ibid.* **62** (1979) 564.
49. S. J. BENNISON and M. P. HARMER, *ibid.* **66** (1983) C90.
50. M. KINOSHITA, *Yogyo-Kyokaishi* **82** (1974) 295.
51. J. RODEL and A. M. GLAESER, *J. Am. Ceram. Soc.* **73** (1990) 3292.
52. A. MOCELLIN and W. D. KINGERY, *ibid.* **56** (1973) 309.
53. Y. FINKELSTEIN, S. M. WIEDERHORN, B. J. HOCKEY, C. A. HANDWERKER and J. E. BLENDELL, in "Symposium on Sintering of Advanced Ceramics" edited by C. A. Handwerker, J. E. Blendell and W. A. Kaysser, (The American Ceramic Society, Cincinnati, Ohio, 1988), Vol. 7, p. 258.
54. J. BLENDELL, W. CARTER and C. HANDWERKER, *J. Am. Ceram. Soc.* **82** (1999) 1889.
55. Y. K. SIMPSON and C. B. CARTER, *ibid.* **73** (1990) 2391.
56. N. RAVISHANKAR and C. B. CARTER, *J. Mater. Res.* **17** (2002) 98.
57. *Idem*., *Inter. Sci.* **8** (2000) 297.
58. D.-Y. KIM, S. M. WIEDERHORN, B. J. HOCKEY, C. A. HANDWERKER and J. E. BLENDELL, *J. Am. Ceram. Soc.* **77** (1994) 444.
59. N. RAVISHANKAR, S. R. GILLISS and C. B. CARTER, *Microsc. Microanal.* **8** (2002) 257.
60. P. L. FLAITZ and J. A. PASK, *J. Am. Ceram. Soc.* **70** (1987) 449.
61. F. UENO and A. HORIGUCHI, in "Euro-Ceramics," edited by G. De, R. A. Tepestra and R. Metselaar, (Elsevier Applied Science, 1992) Vol. 1, p. 1.383.
62. J. DRENNAN, D. R. CLARKE, R. H. J. HANNINK and T. M. SHAW, *J. Am. Ceram. Soc.* **77** (1994) 2001.
63. V. G. LEVICH and V. S. KRYLOV, *Ann. Rev. Mater. Sci.* **1** (1969) 293.
64. S. RAMAMURTHY, C. B. CARTER and H. SCHMALZRIED, *Phil. Mag.* **80** (2000) 2651.
65. W. W. MULLINS, *Acta Metall.* **6** (1958) 414.
66. C. L. DI PRINZIO and O. B. NASELLO, *Scripta Mater.* **39** (1998) 1617.
67. V. Y. ARISTOV, V. Y. FRADKOV and L. S. SHVINDLERMAN, *Phys. Metal. Metall.* **45** (1978) 83.
68. N. E. MUNOZ, S. R. GILLISS and C. B. CARTER, *Phil. Mag. Lett.* **84** (2004) 21.
69. I. MANASSIDIS and M. J. GILLAN, *J. Am. Ceram. Soc.* **77** (1994) 335.
70. H. SUZUKI, H. MATSUBARA, J. KISHINO and T. KONDO, *J. Ceram. Soc. Japan* **106** (1998) 1215.
71. D. E. ELLIS, J. GUO and D. J. LAM, *J. Am. Ceram. Soc.* **77** (1994) 398.
72. M. CAUSA, D. R. C. PISANI and C. ROETTI, *Surf. Sci.* **215** (1989) 259.
73. W. C. MACKRODT, R. J. DAVEY, S. N. BLACK and R. DOCHERTY, *J. Crystal Growth* **80** (1987) 441.
74. P. W. TASKER, in "Structure and Properties of MgO and Al_2O_3," edited by W. D. Kingery, Vol. 10 (American Ceramics Society, 1984) p. 176.
75. M. KITAYAMA and A. M. GLAESER, *J. Am. Ceram. Soc.* **85** (2002) 611.
76. J.-H. CHOI, D.-Y. KIM, B. J. HOCKEY, S. M. WIEDERHORN, C. A. HANDWERKER, J. BLENDELL, W. C. CARTER and A. R. ROOSEN. *ibid.* **80** (1997) 62.
77. M. P. MALLAMACI and C. B. CARTER, *Acta Mater.* **46** (1998) 2895.
78. J. K. FARRER, N. RAVISHANKAR, J. R. MICHAEL and C. B. CARTER, *Microsc. Microanal.* **7** (2001) 326.
79. J. K. FARRER, J. R. MICHAEL and C. B. CARTER, in "Electron Backscatter Diffraction in Materials Science," edited by A. J. Schwartz, M. Kumar and B. L. Adams (Plenum, 2000) p. 299.
80. J. R. MICHAEL, in "Elec. Back. Diff. Mater. Sci.," edited by A. J. Schwartz, M. Kumar and B. L. Adams (Kluwer Academic/Plenum Publishers, 2000) p. 75.
81. M. P. MALLAMACI, J. BENTLEY and C. B. CARTER, *Acta Mater.* **46** (1997) 283.
82. J. R. MICHAEL and R. P. GOEHNER, in "52nd Annual Meeting Microscopy Society of America," edited by G. W. Bailey and A. J. Garratt-Reed (San Fancisco Press, Inc., New Orleans, LA, 1994) p. 596.
83. R. P. GOEHNER and J. R. MICHAEL, *J. Res. Nat. Inst. Standard. Techn.* **101** (1996) 301.
84. B. L. ADAMS, S. I. WRIGHT and K. KUNZE, *Metall. Trans. A—Phys. Metall. Mater. Sci.* **24** (1993) 819.
85. J. R. HEFFELFINGER, M. W. BENCH and C. B. CARTER, *Surf. Sci.* **343** (1995) L1161.
86. J. R. HEFFELFINGER and C. B. CARTER, *ibid.* **389** (1997) 1.